ACS OMEGA

Open Access

http://pubs.acs.org/journal/acsodf

Article

Graphene Oxide Enhanced Monoethanolamine and Ethylenediamine Nanofluids for Efficient Carbon Dioxide Uptake from Flue Gas

Nomcebo P. Khumalo, Oranso T. Mahlangu, Bhekie B. Mamba, and Machawe M. Motsa*

Cite This: *ACS Omega* 2024, 9, 25625−25637

Read Online

ACCESS | Metrics & More | Article Recommendations

ABSTRACT: The addition of nanoparticles in amine solutions to produce a stable amine-based nanofluid provides a high surface area for absorption and improves the absorption rate. In this work, nanofluids were prepared by dispersing graphene oxide (GO) in monoethanolamine (MEA) and ethylenediamine (EDA) solutions for adsorption of carbon dioxide (CO_2) to further improve their absorption performance by providing more reaction sites on the GO framework. GO was synthesized using the modified Hummers method and characterized for physicochemical properties using SEM, EDS, FTIR, Raman analysis, and TGA. The FTIR spectra for the GO nanoparticles before absorption showed peaks attributed to C−C, H−C, and C−O bonding. After the absorption experiments, the FTIR spectra of GO showed peaks due to C−O−NH_2, N−O−N, and N−H bonding. The BET analysis further confirmed the decrease in the surface area, pore volume, and pore diameter of the GO recovered from the nanofluids after the CO_2 experiment, indicating an interaction between GO and amine molecules. The absorption process of CO_2 by the nanofluid was performed in a custom-made pressure chamber whereby the CO_2 gas was in direct contact with the absorption fluids. The obtained adsorption rate constant (k) for the reaction between CO_2 and 30% MEA and EDA solutions was 0.113 and 0.131, respectively. Upon addition of 0.2 mg/mL GO in the base solution, k increased to 0.16854 and 0.17603 for the MEA and EDA nanofluids, respectively. The proposed mechanism involves GO nanoparticles interacting with the amine groups through the oxygen-rich groups of GO. This results in the formation of a zwitterion that readily reacts with CO_2, resulting in a carbamate.

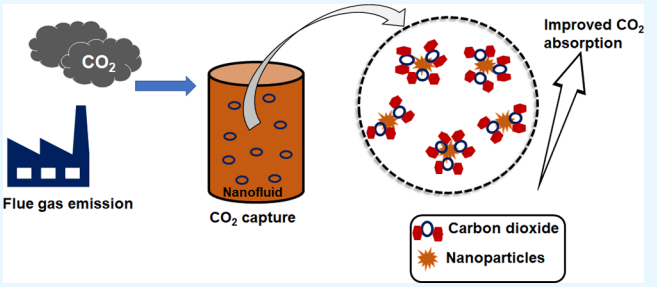

1. INTRODUCTION

1.1. Background. To this date, several innovative carbon dioxide separation technologies have been established including chemical absorption,[1] adsorption,[2] membrane separation,[3] gas−liquid membrane contactors (GLMC),[4−6] chemical looping,[7] cryogenic separation,[8,9] etc. However, the capturing step is complicated and expensive; thus, it has been the focus area for most research studies to develop simpler and cost-effective CO_2 capture techniques.

Most of the absorption liquids such as water and physical absorbents have a low CO_2 absorption efficiency. Therefore, many research outputs have attempted to employ chemical absorbents as additives to physical absorbents to increase their absorption efficiency for the targeted gases. One advantage of physical absorption as opposed to chemical absorption is the low energy requirement during regeneration and the absence of corrosion or oxidative degradation on the membrane surface.[10] Nonetheless, chemical absorption has remained a commonly used technique due to its high absorption performance. In chemical absorption, liquids such as liquid amines,[11] electrolytes, ionic liquids,[12] and now recently, nanofluids[13] can be used for CO_2 absorption to solutions.

Nanomaterials such as zeolites[14] and carbon-based materials[15,16] have attracted attention in CO_2 adsorption, storage, and separation because they provide a high surface area for adsorption, are easily available due to industrial scale synthesis, and possess excellent chemical and thermal stability. Graphene oxide has been reported as an efficient adsorbate for acid gases due to the high surface area it provides and stable chemical structure.[17] Some researchers have investigated the physisorption of CO_2 on graphene oxide (GO),[18] reduced graphene oxide (rGO),[19] and amine-functionalized graphene oxide.[20,21] One advantage of the GO structure is that it consists of oxygen-rich groups such as hydroxide and epoxide groups

Received: August 28, 2023
Revised: February 1, 2024
Accepted: February 13, 2024
Published: June 5, 2024

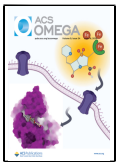

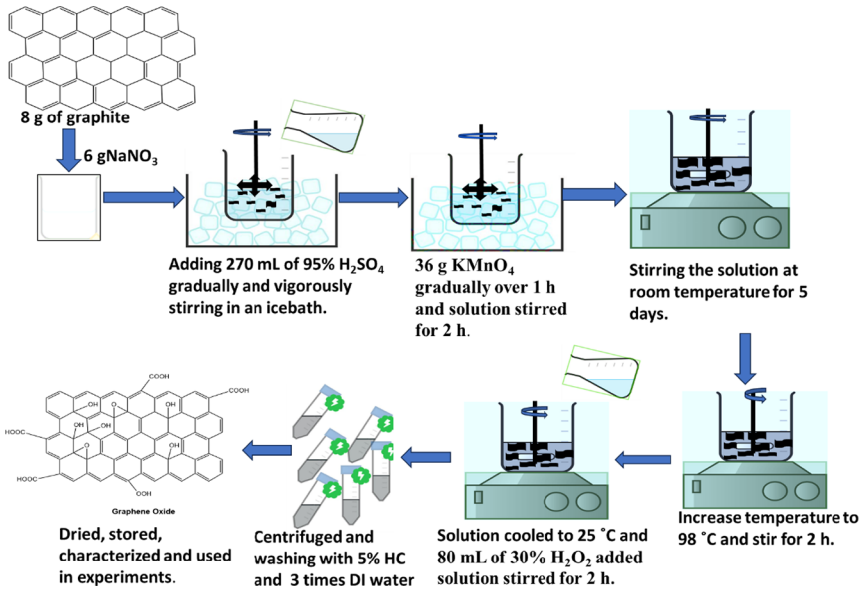

Figure 1. Illustration diagram showing synthesis of graphene oxide using a modified hummers method.

attached to the surface and carboxyl and carbonyl groups on the edges. These oxygen-rich functional groups are the common reaction sites for a wide range of chemical reactions.[22]

A nanofluid can be defined as a fluid that has nanoparticles below 100 nm diameter stably dispersed in a base liquid to form a stable colloidal suspension.[23] The synthesis process and stability of the nanofluids are important factors that contribute to the performance potential of the nanofluid. Several studies have employed nanofluids for the uptake of carbon dioxide. The mechanism of enhanced absorption performance in nanofluids has not been clearly established. Yu et al.[23] studied the enhancement of CO_2 uptake in water-based nanofluids with stably dispersed carbon nanotubes. The authors attributed the increase in the CO_2 absorption of the nanofluids to the improvement in the convective movement due to Brownian motion and the shuttle effect.

Irani et al.[24] investigated the absorption of CO_2 in GO/methyldiethanolamine (MDEA) nanofluid whereby 0.1 and 0.2 mg/mL of GO were dispersed in 40% MDEA by ultrasonication. The obtained results indicated that the dispersion of GO in MDEA enhanced the absorption capacity by 9.1% compared to CO_2 absorption by 40% MDEA solution without the nanoparticles. The experiments further found that the CO_2 uptake capacity of the nanofluid declined with an increase in temperature and increased with increasing pressure. The authors attributed the improvement of the CO_2 absorption capacity to the hydrodynamic effects in which nanoparticles reduced the gap between the gas−liquid interface due to collisions.

Other studies cited the hydrodynamic effects, whereby the presence of the nanoparticles effected convective mobility at the gas−liquid interface. Therefore, increasing the mass transfer through the liquid improves the absorption performance. Pashaei and Ghemei[25] recommended a loading of 0.1 wt % ZnO nanoparticles in diethanolamine (DEA) solution for a high yield of hydrodynamic effect and absorption performance in a stirrer bubbler column of 33.3%. The absorption performance in a stirrer bubbler column of TiO_2 and ZrO_2 was 35 and 23%, respectively, at 0.05 wt % loading in DEA solution, implying a high yield of hydrodynamic effect at low percentage loading.

Therefore, nanoparticle loading in nanofluids is another factor that influences the hydrodynamic and absorption phenomena. Rahmatmand and coauthors[26] investigated the CO_2 absorption improvement by SiO_2, Al_2O_3, Fe_3O_4 and magnetic carbon nanotubes MCNTs nanofluids based on water and 5% DEA and 5% methyldiethanolamine (MDEA) solutions to form concentrations of 0.02, 0.05, and 0.1 wt %. The authors reported that SiO_2 and Al_2O_3 showed increased performance at high concentrations (0.1 wt %) and enhanced the absorption performance by 2 and 18%, respectively. On the other hand, MCNT and Fe_3O_4 were effective at loading of 0.02 wt % enhancing the absorption performance by 34 and 24%, respectively. The authors attributed the difference in the kinetics of the nanofluids during absorption to the different surface areas provided by the nanoparticles.

Devakki and Thomas[27] investigated 0.02−0.14 wt % of TiO_2 and Al_2O_3 water-based nanofluids CO_2 uptake performance. It was observed that an increase in the nanoparticle loading of the nanofluid resulted in improved CO_2 absorption performance. This was attributed to the increase in surface area provided by the nanoparticles in the nanofluid. However, further loading of the nanoparticles decreases the viscosity of the nanofluid resulting in low mass transfer from the restricted Brownian motion. Therefore, the absorption efficiency of CO_2 is reduced at higher nanoparticle loading.

Current research projects are in pursuit of a CO_2 absorbent with a high absorption capacity, low cost, ease of regeneration, and high affinity for carbon dioxide. Available research on nanofluids has not yet provided information on the selectivity of the nanofluids. The selectivity of amine solutions toward carbon dioxide has been demonstrated.[28] Graphene oxide is a versatile nanoparticle with a tunable layer structure providing a platform for a wide range of chemical reactions.[29] Due to its hydrophilic nature, graphene oxide can be easily dispersed in water and several solvents, thus providing compatibility with water and alkanolamine solutions. Graphene oxide-amine liquid nanofluids have good potential in the upgrading of

https://doi.org/10.1021/acsomega.3c06425
ACS Omega 2024, 9, 25625−25637

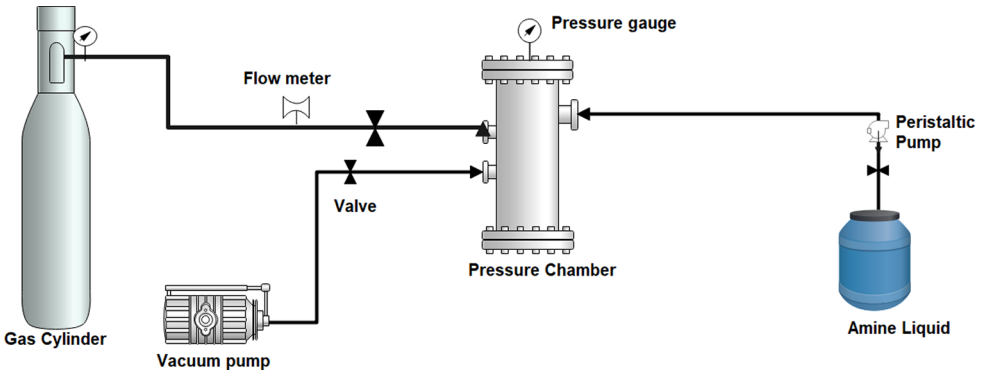

Figure 2. Illustration diagram showing the chemical absorption experiment setup.

biogas. However, the selectivity of GO-based nanofluids to carbon dioxide has not been fully demonstrated.

This work seeks to highlight the effect of incorporating graphene oxide nanoparticles in amine liquids to improve the absorption of carbon dioxide (CO_2). Through the help of characterization techniques, the study proposes an absorption mechanism of how the GO interacts with the amine liquids used: monoethanolamine (MEA) and ethylenediamine (EDA). To investigate the effect of suspending GO in primary and secondary amines. Furthermore, the study investigates the absorption of CO_2 in the presence of methane gas (CH_4). Lastly, the regeneration and reuse of the regenerated and cyclic capacities of the liquid absorbent are investigated.

2. MATERIALS AND METHODS

2.1. Materials Used. The chemicals used in this study were procured from Sigma-Aldrich, Johannesburg, South Africa. The chemicals were reagent grade and included sodium nitrate ($NaNO_3$) 99.99%, graphite 99.99% natural, potassium permanganate ($KMnO_4$) 99.99%, sulfuric acid (H_2SO_4) 95.0−98.0%, monoethanolamine (MEA) 99.99%, ethylenediamine (EDA) 99.99%, and hydrogen peroxide (H_2O_2) 34.5−36.5%. Deionized water (DI water), obtained from a Milli-Q system (Millipore, USA), was used in all experiments reported in this work. Carbon dioxide (CO_2) gas cylinder (98% purity) and methane (CH_4) gas cylinder (98% purity) were purchased from Afrimax, South Africa.

2.2. Synthesis of Graphene Oxide. For the preparation of graphene oxide (GO), the modified Hummers method was used[30] (see Figure 1). During the preparation, 8 g of graphite, a precursor material, and 6 g of $NaNO_3$ were weighed and transferred into a 1 L beaker. The beaker was inserted in an ice bath to reduce the reaction temperature; then 270 mL of 95% H_2SO_4 was added gradually and vigorously stirred. Then 36 g of $KMnO_4$ was gradually obtained over a time frame of 1 h. The mixture was continuously stirred in an ice bath for 2 h. The mixture was taken off from the ice bath and stirred at room temperature for 5 days to facilitate complete oxidation. After 5 days of the oxidation process, 400 mL of 5% H_2SO_4 was added dropwise to the mixture over a period of 1 h. The temperature of the reaction steadily increased from room temperature to 98 °C in 1 h. The reaction was then stirred at 98 °C for 2 h before cooling the temperature to 25 °C. Upon reaching room temperature, 80 mL of 30% H_2O_2 was added into the reaction, and the mixture was stirred for 2 h. Theoretically, the H_2O_2 reacted with excess $KMnO_4$. The mixture was centrifuged at 3 372 rpm for 20 min to separate GO, and then it was rinsed repeatedly using 5% HCl and rinsed with DI water to remove impurities. Then the GO was dried in the oven at 60 °C for 18 h and characterized using different physicochemical properties.

2.3. Synthesis of Nanofluids. Nanofluids were prepared by suspending GO nanoparticles in two base solutions, 30% monoethanolamine (MEA) and ethylenediamine (EDA). The content of GO was varied to obtain nanofluids with concentrations of 0−0.5 mg/mL GO. After suspension, the solutions were sonicated for 2 h using an Elma ultrasonic cleaner s100h sonicator at room temperature (25 °C) at 37 kHz ultrasonic frequency to allow uniform dispersion of the nanoparticles.

2.4. Characterization of Graphene Oxide and Nanofluids. Graphene oxide was characterized using Fourier transform infrared (FTIR, PerkinElmer, Massachusetts, USA) and Raman spectroscopy (Raman Micro 200 spectrometer, PerkinElmer, USA), and size and charge were measured using Malvern Zetasizer (Malvern, U.K.). Scanning electron microscopy (SEM) (JEOL, Japan JSM−IT300) coupled with an energy-dispersive X-ray spectroscopy detector (EDS, Oxford Instruments, U.K.) was used for morphology properties and elemental analysis of GO nanoparticles. Prior to the analysis using SEM and EDS, the nanoparticles were coated with gold (Q150R ES, Quorum Technologies, U.K.). Thermogravimetric analysis (TGA) was used to determine the thermal stability of the nanoparticles. BET analysis of the GO nanoparticles was conducted using a Quanta-chrome Autosorb iQ3 Automated gas sorption analyzer (Austria, Anton Paar, GmbH, Graz).

2.5. Bench-Scale CO_2 Absorption. The uptake of CO_2 by the nanofluid was performed in a custom-made pressure chamber (300 mL) whereby the CO_2 gas was in direct contact with 100 mL of the absorption liquids. The pressure decay experiments were performed in triplicates. Then the averages were used to calculate the Moles absorbed (mol/kg), absorption constant (k), and solubility (x). Before carbon dioxide gas was introduced into the chamber, a vacuum pump was used to remove any present gases. Different parameters such as type of nanofluid, concentration of GO (0−0.5 mg/mL), carbon dioxide absorption kinetics, and CO_2 solubility were studied. The base solutions were 30% MEA and EDA solutions. The effect of mixed gas during absorption of carbon dioxide was also studied using the amine liquids and best-performing nanofluids. The base and best-performing nanofluids were regenerated by desorbing CO_2 gas at 90 °C for 2h. The increase in the heat loosens the bond between the CO_2 and amine groups. The mechanism of CO_2 absorption by the

https://doi.org/10.1021/acsomega.3c06425
ACS Omega 2024, 9, 25625−25637

nanofluids was proposed from the results, and the findings of this work provide valuable insights into the future use of nanofluids for CO_2 absorption. The bench-scale experimental setup is demonstrated as a schematic diagram shown in Figure 2.

The absorption of CO_2 during the experiments was defined by eq 1.

$$\propto = \frac{\left[\frac{V_{gas}}{Rx298}\left(\frac{P_0}{Z_0} - \frac{P_n}{Z_n}\right)\right]}{V_{liq}P_{liq}} \quad (1)$$

whereby α (mol/kg) is the absorbed CO_2; V_{gas} (cm^3) and V_{liq} (cm^3) are described as the gas volumes; and P_{liq} ($kg.cm^{-3}$) is the density of the nanofluid. R (kPa cm^3 K^{-1} mol^{-1}) is the universal gas constant at 298 K. P_0 (kPa) and P_n (kPa) are the initial pressure and pressure at any given time, respectively. Finally, Z_0 and Z_n are the compressibility factors at the initial time and any given time, computed using the Redlich−Kwong equation of state.

Using the moles of CO_2 gas absorbed, the solubility of the CO_2 in the different solutions was calculated as expressed by eq 2.

$$x = \frac{V(\text{STP})\text{of absorbed gas}}{\text{solvent volume}} \quad (2)$$

Equation 3 was used to calculate the rate of mass transfer of CO_2 into the liquid phase:[31]

$$\frac{n_t}{n_\infty} = kt^{0.5} \quad (3)$$

whereby k is defined as an adsorption rate constant, and t is the time in min k was estimated from the slope of the graph of n_t/n_∞ versus $t^{0.5}$.

To calculate the percentage enhancement attributed to the addition of nanoparticles in the absorbent liquid (%E), eq 4 was used.

$$\%E = \frac{CO_2 \text{ absorption rate in nanofluid} - CO_2 \text{absorption rate in base fluid}}{CO_2 \text{ absorption rate in base fluid}} \times 100 \quad (4)$$

2.6. Regeneration Studies. The regeneration of the solutions was undertaken in a water bath at 90 °C for 2 h to release absorbed CO_2. After each CO_2 absorption, the amine solutions and amine-based nanofluids were introduced into a three-necked flask and then into the heated water bath to initiate the desorption. Then the regenerated as used in the CO_2 absorption experiment for 3 cycles.

3. RESULTS AND DISCUSSION

3.1. Fourier Transform Infrared (FTIR) Spectroscopy. The functional groups of GO and different oxygen functionalities were identified by using FTIR spectroscopy (Figure 3a). The GO nanoparticles showed an apparent absorption peak at 3250 cm^{-1} which was due to vibrational modes of the hydroxyl functional group (O−H). The carbonyl group (C═O) absorbed at 1733 cm^{-1}, sp^2 hybridized C═C (in-plane stretching) at 1622 cm^{-1}, alkoxy group at 1260 cm^{-1}, and epoxy group at 1047 cm^{-1}.[32] The FTIR spectra confirmed the successful synthesis of GO nanoparticles.

In Figure 3b, the FTIR spectra of GO recovered from amine nanofluids after the absorption experiment has been conducted can be observed. GO was sieved out from the nanofluids, dried,

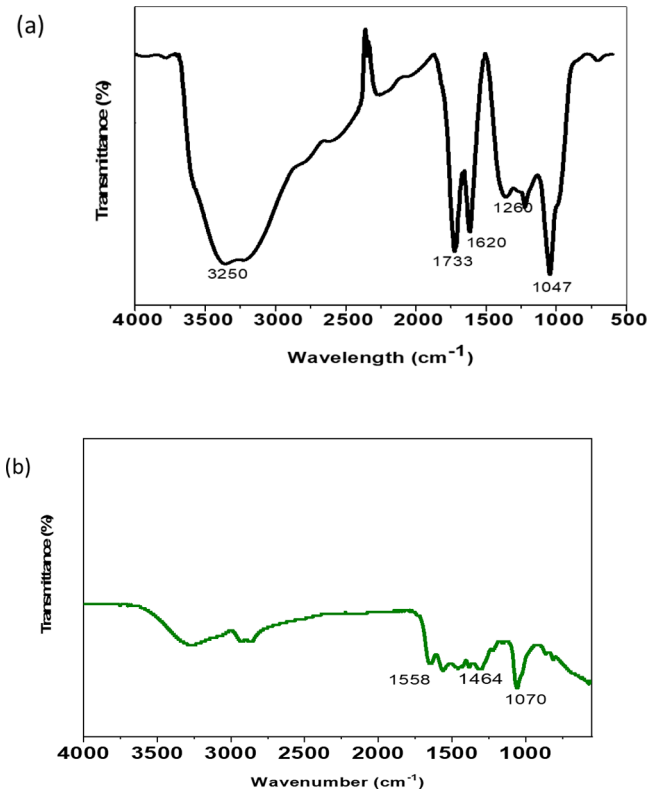

Figure 3. (a) FTIR spectroscopy for GO nanoparticles. (b) FTIR spectroscopy for GO nanoparticles after absorption experiments.

and analyzed. It can be observed that peaks attributed to oxygen disappear while a new band at 1558 cm^{-1} attributed to N−O−N, another band at 1464 cm^{-1} corresponded to N−H plane stretching, and a band at 1070 cm^{-1} attributed to C−N.[33]

3.2. Raman Spectroscopy. Raman spectroscopy is considered as one of the simplest and invasive techniques used for the characterization of carbon-based materials because of the presence of conjugated and double carbon−carbon (C═C) bonds. Figure 4 presents Raman spectroscopy of GO

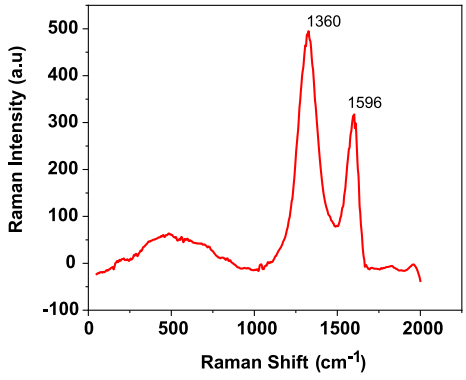

Figure 4. Raman spectroscopy of the GO nanoparticles.

whereby the G peak at 1596 cm^{-1} and the D peak at 1400 cm^{-1} were observed. The G-band is due to the graphitic carbon (C) in GO, while the D-band is linked to defects in the graphitic domain.[34] The G and D bands occur because of first-order scattering from the E2g phonon of sp^2 C atoms.[35]

https://doi.org/10.1021/acsomega.3c06425
ACS Omega 2024, 9, 25625−25637

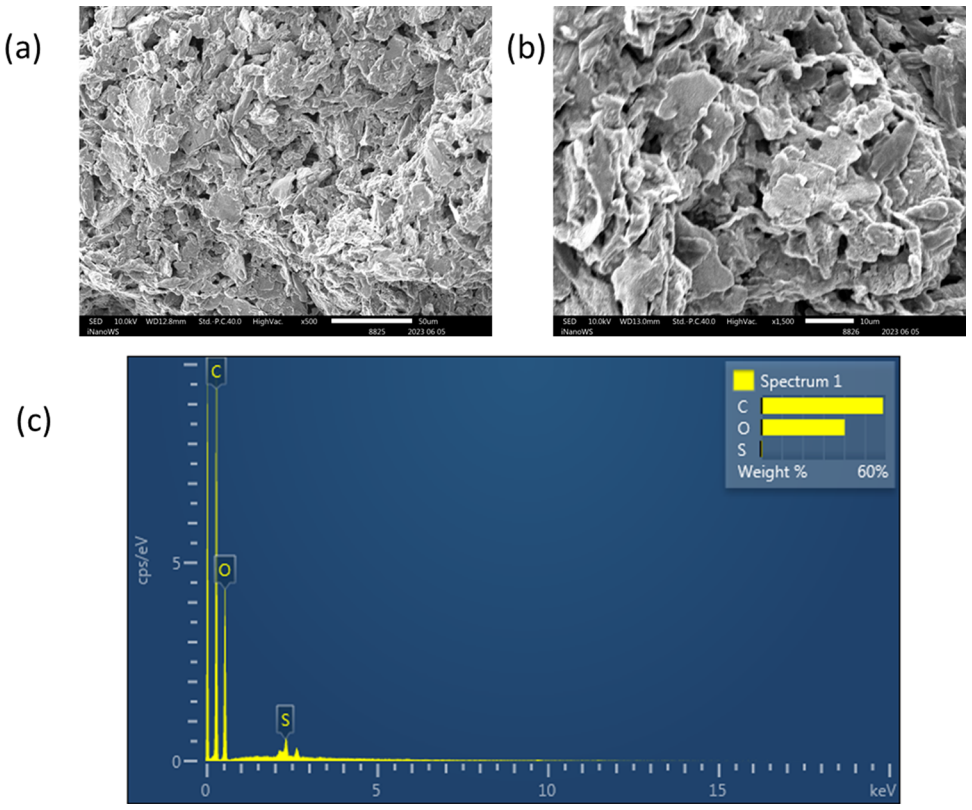

Figure 5. SEM images and EDS spectra for GO nanoparticles: (a) SEM image observed area 50 μm, (b) SEM image observed area 10 μm, and (c) EDS spectra of the nanoparticles.

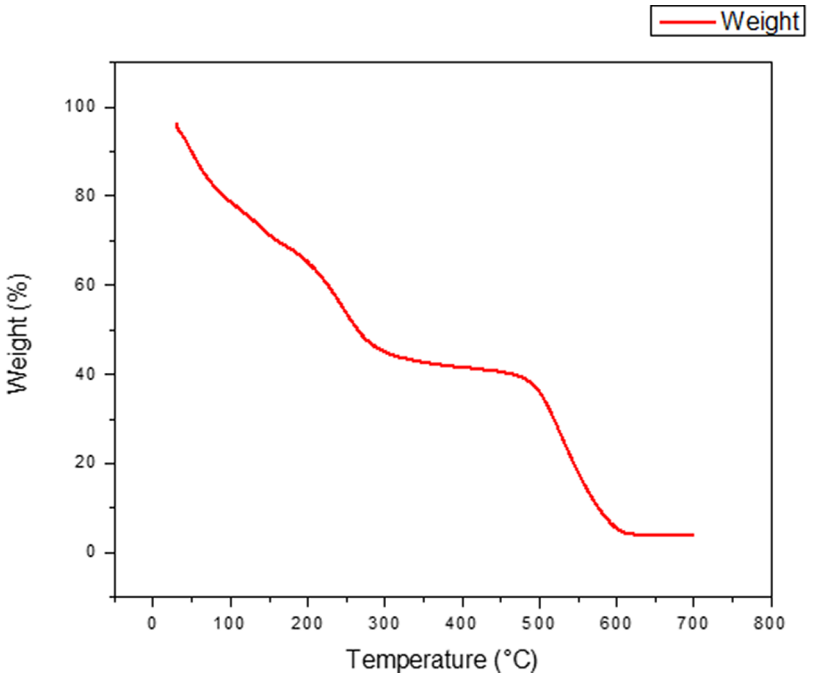

Figure 6. TGA analysis of graphene oxide.

3.3. Scanning Electron Microscopy and Energy-Dispersive X-ray Spectroscopy Studies. Scanning electron microscopy (SEM) was used to observe the GO nanoparticle surface morphology. Figure 5 displays a layered structure of GO with curved edges, and pores in the interface of these layers could be observed. These features show that the GO has a large surface area which is a desired property for absorption. Energy-dispersive X-ray spectroscopy (EDS) was used to analyze the elemental composition of GO. Figure 5c confirms the presence of C and O, which are the main elements found in GO. The low content of sulfur may be attributed to traces from sulfuric acid used during the synthesis. No other elements

https://doi.org/10.1021/acsomega.3c06425
ACS Omega 2024, 9, 25625−25637

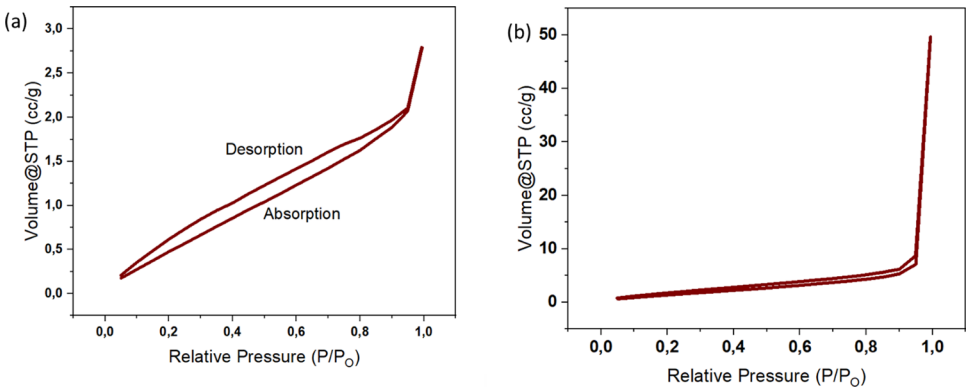

Figure 7. Nitrogen absorption and desorption isotherm curves of (a) fabricated graphene oxide and (b) graphene oxide recovered from amine liquids after the CO_2 absorption experiments.

or impurities were detected showing that GO of acceptable purity was synthesized.

3.4. Size and Charge of Graphene Oxide. The zeta potential of nanoparticles is considered to be an important parameter in characterizing the stability of the nanoparticles in dispersion in water or solutions.[36] The zeta potential measures the charge of the electric double layer around colloidal particles because of ionization of different functional groups in the solution. Generally, nanoparticles with a zeta potential in the range of −35 to 30 mV are considered stable due to electrostatic repulsion.[37,38] The average measured zeta potential for fabricated GO was ± −9.66 mV.

3.5. Thermogravimetric Analysis. Thermogravimetric investigation of GO was undertaken in a nitrogen environment. Figure 6 shows the thermogravimetric decay of GO due to a temperature increase. Graphene oxide experiences a weight loss from 50 to 200 °C owing to evaporation of absorbed water molecules. The first curve stage, around 100 °C with low weight loss (10%) was attributed to the loss of entrapped water molecules. The second loss occurring at 256 °C (with a weight loss of 23%) was due to the removal of oxygen-containing molecules in the GO. At 586 °C, there was a high loss of about 57% due to the pyrolysis of CO and CO_2 and decomposition of the ring carbon. The observed degradation stages were also obtained in different studies by Sadhukhan et al.[39] and Alshamsi et al.[40] Due to the high temperature required to decompose functional groups during thermal analysis, it can be derived that the nanoparticles structurally remain stable at the temperature of 180 °C. This can accommodate regeneration of the nanofluid by releasing CO_2 in a heat-driven process at temperatures of 100−135 °C.

3.6. Brunauer−Emmett−Teller (BET) Analysis for Graphene Oxide. The Brunauer−Emmet−Teller (BET) analysis utilizing the nitrogen or argon adsorption−desorption isotherm is a common technique used to determine the surface area, pore diameter, and pore volume of porous nanomaterials.[41,42] The BET technique was used to analyze the surface area of the fabricated GO and the GO recovered from the amine-based nanofluids. The obtained nitrogen absorption and desorption curves are shown in Figure 7. The absence of the hysteresis split (lag-loop) between the absorption and desorption curves indicates that the mesoporous pores of the recovered GO have been filled up due to amine−GO interaction (Figure 7b). On the other hand, the existence of the hysteresis split in the fabricated GO from 0.1 to 0.98 P/P_0 indicates that initially, the GO had mesoporous pores which were then depleted due to the GO−amine interaction. It can also be observed that nitrogen uptake of the fabricated GO was steeper than the GO recovered from the nanofluids, confirming that a high number of micropores were present before the interaction with amine liquid.

The difference in surface area, pore volume, and pore diameter of the fabricated GO and GO sieved out from nanofluids after CO_2 absorption is displayed in Table 1. The

Table 1. Surface Area, Pore Volume, and Pore Diameter of Graphene Oxide before and after CO_2 Absorption

type	surface area S_{BET}	pore volume	pore diameter
GO	240.776 m^2/g	0.075 cc/g	3.406 nm
recovered GO	31.946 m^2/g	0.051 cm^3/g	1.941 nm

observed decrease in surface area, pore volume, and pore diameter indicates that the GO interacted with the amine molecules forming a zwitterion, and this results in the amine molecules occupying the pores of graphene oxide.

3.7. Carbon Dioxide Absorption Using Amine-Based Nanofluids. Figure 8a shows the pressure decay during carbon dioxide absorption by the MEA solution and MEA-based nanofluid. It can be observed that the reached state of equilibrium increased with increasing nanoparticle loading, then decreases for the nanofluids with 0.4 and 0.5 mg/mL GO dispersed in both solutions. Figure 8b shows kinetics of the CO_2 absorption experiment in moles of CO_2 absorbed against time. It can be observed that the moles of the CO_2 absorption rate are evidently faster for the nanofluids with 0.1, 0.2, and 0.3 mg/mL GO nanoparticles and slower for the nanofluids with 0.4 and 0.5 mg/mL GO nanoparticles (Figure 8b). The increase in kinetics can be explained by the additional surface area provided by the GO nanoparticles. However, further loading, increased the viscosity of the nanofluid, thus becoming bulkier which restricts Brownian motion.[27] The decrease in absorption rate due to further nanoparticle loading can also be attributed to agglomeration of nanoparticles, thus decreasing the surface area.

Figure 9a,b shows the pressure decay during carbon dioxide absorption and CO_2 uptake kinetics by the EDA solution and EDA-based nanofluids. It can be observed that the nanofluids with 0.1 0.2, and 0.3 mg/mL reached the state of equilibrium faster as compared to the 30% EDA solution. It can be observed that EDA solution. The CO_2 absorption behavior of EDA solution and EDA-based nanofluids can be considered

https://doi.org/10.1021/acsomega.3c06425
ACS Omega 2024, 9, 25625−25637

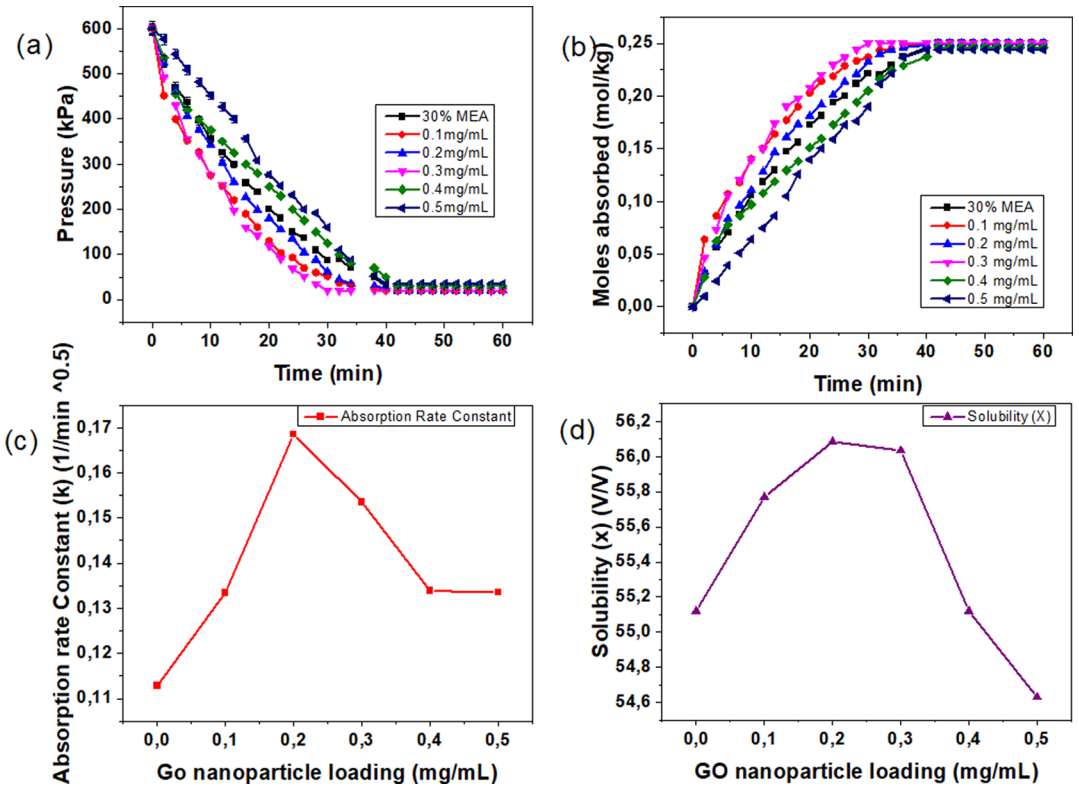

Figure 8. Effect of nanoparticles in 30% MEA solution on absorption of CO_2 on (a) pressure decay, (b) moles absorbed, (c) absorption rate constant, and (d) solubility.

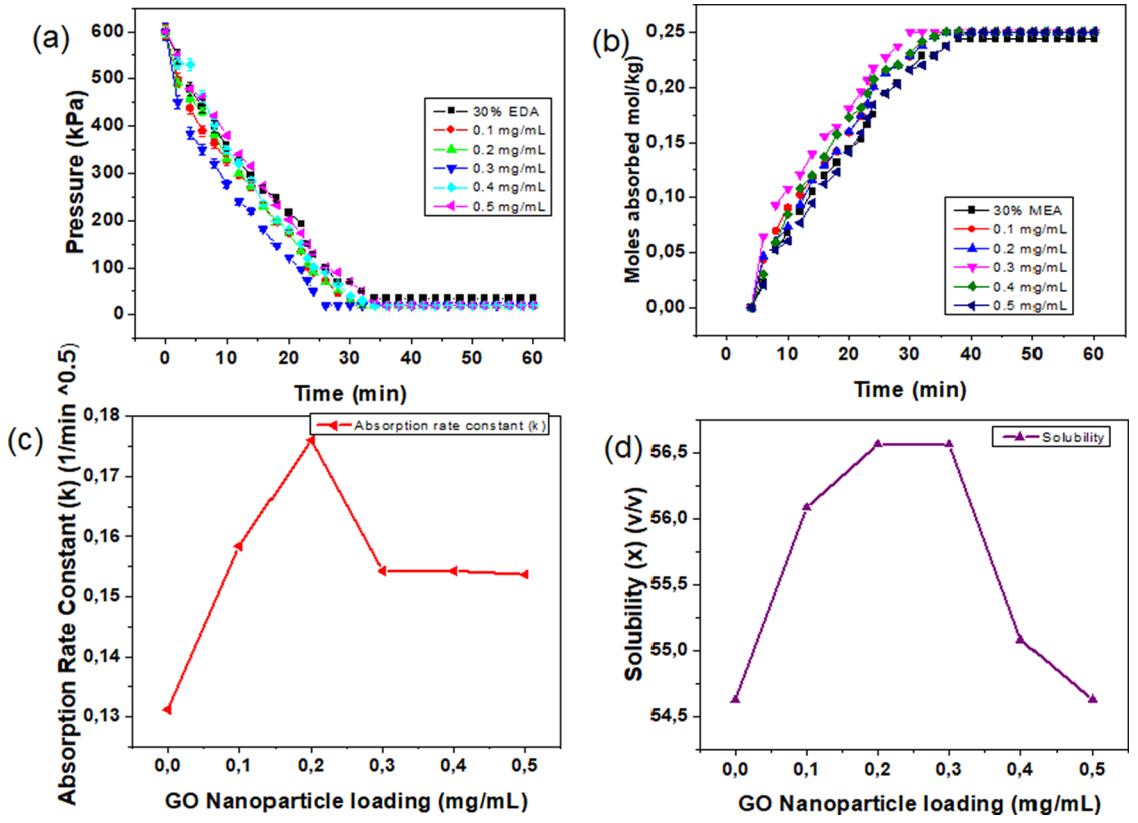

Figure 9. Effect of nanoparticles in 30% EDA solution on absorption of CO_2 on (a) pressure decay, (b) moles absorbed, (c) absorption rate constant, and (d) solubility.

https://doi.org/10.1021/acsomega.3c06425
ACS Omega 2024, 9, 25625−25637

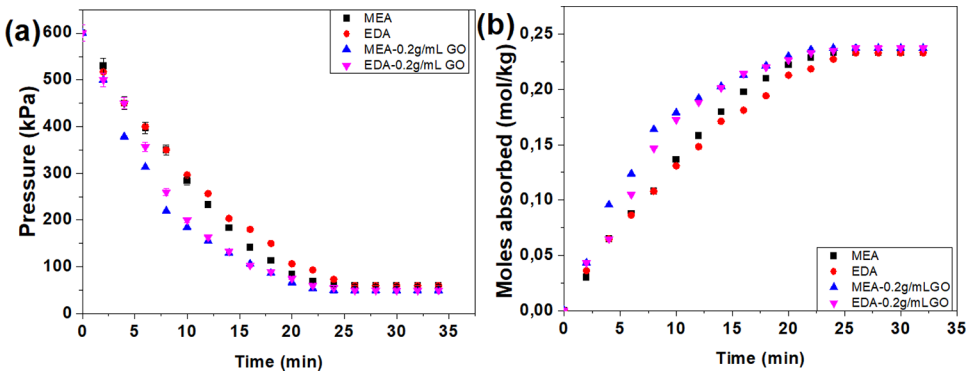

Figure 10. (a) Pressure decay and (b) absorption kinetics of CO_2 during the 50/50 binary CH_4/CO_2 gas system.

similar to that of the MEA solution and MEA-based nanofluids. This is because both the MEA-based solution/nanofluids and EDA-based solutions/nanofluids reach close values for the CO_2 loading. This behavior can be attributed to with low degree of carbamate hydrolysis during the CO_2 absorption experiments and hindering improvement in CO_2 loading in the solutions.[43]

The CO_2 absorption rate constant of the nanofluid was calculated from the kinetics. It was observed that the CO_2 absorption rate constant of the EDA base fluid was higher as compared to that of the MEA base solution: 0.13119 and 0.11285 (1/min^0.5), respectively. This can be attributed to an observation made by Sharma that the absorption rate of CO_2 in EDA is higher than that of MEA at low amine concentrations and low CO_2 concentrations.[44] The highest absorption rate obtained for the MEA and EDA-based nanofluids with 0.2 mg/mL GO loading was 0.16854 and 0.17603 (1/min^0.5), respectively. Therefore, the enhancement factor of the CO_2 absorption rate for nanofluid with 0.2 mg/mL GO nanoparticles in the MEA solution was 49%. The enhancement factor due to 0.2 mg/mL GO nanoparticles in the EDA solution was 34%. The GO nanoparticles have high surface area and available active sites as platforms for a wide range of chemical reactions thus resulting in an improvement of the absorption rate.[24] Ghasemi et al. synthesized amino-functionalized ZIF-90@GO/MDEA nanofluid for carbon dioxide absorption and obtained 23% enhancement in the absorption rate when 0.1 wt % amino-functionalized ZIF-90@GO was added in 40 wt % MDEA.[45] The authors attributed the enhancement in absorption rate to the available active site of the nanoparticles. However, the authors did not support their finding by further characterization of the nanoparticles after the absorption experiment.

The solubility of CO_2 in amine-based nanofluids was observed to increase with increasing GO nanoparticle loading. However, at higher GO loadings of 0.4 and 0.5, the solubility decreased, as depicted in Figures 7d and 8d. In the MEA-based nanofluid, the highest CO_2 solubility increase obtained was for the 0.2 mg/mL GO loading of 56.0849 v/v, while the base CO_2 in the 30% MEA base fluid was 55.12 v/v. Therefore, the highest increase observed in CO_2 sorption was 1.73% due to the GO nanoparticle. On the other hand, the CO_2 solubility of the 30% EDA base fluid was 54.63, and the highest obtained solubility after loading of GO was 56.562 for both 0.2 and 0.3 mg/mL nanofluids. This was an increase of 3.64% of the CO_2 sorption due to GO nanoparticles. This trend was concurrent with results obtained by Mohammadpour et al.[31] and Irani et al.,[24] where the authors investigated the influence of dispersing GO in monoethanolamine and methyl diethanolamine, respectively.

3.8. Reaction Mechanisms. Theoretically, in an amine solution, CO_2 reacts with the amine group (symbolized as AmH), hydroxide ion (OH^-) and water (H_2O) to form a stable carbamate. The reaction equations (eqs 5−7) show the absorption mechanism in amine solutions:[46]

$$CO_2 + 2AmH \leftrightarrow AmCOO^- + AmH^+ \quad (5)$$

An unstable carbamate readily undergoes hydrolysis, forming bicarmate and releasing unbonded amine molecules:

$$AmCOO^- + H_2O \leftrightarrow AmH + HCO_3^- \quad (6)$$

In low amine concentrations, the interaction between CO_2 and amine is slow; therefore, the following equation becomes predominant:

$$CO_2 + AmH + H_2O \leftrightarrow AmH_2^+ + HCO_3^- \quad (7)$$

Ethylenediamine (EDA) reacts with CO_2 to produce both monocarbamate and dicarbamate. There are two proposed mechanisms for this reaction: termolecular and zwitterion mechanisms.[46] On the other hand, monoethanolamide reacts with CO_2 to produce monocarbamate using a zwitterion-mediated two-step mechanism to produce a carbamate.[47] Therefore, this research proposes that amine molecules are inserted into the gallery spaces of graphene oxide by interacting with the oxygen-containing groups of graphene oxide through hydrogen bonding, resulting in the protonation of the amine forming a zwitterion as expressed in eq 8.

$$R'R'R' - OH + AMH \leftrightarrow R'R'RO - \acute{A}MH_2^+ \quad (8)$$

The protonated amine group on graphene oxide then reacts with carbon dioxide introduced in the pressure chamber to form a carbamate as shown by eq 9.

$$R'R'R - O - AMH_2^+ + CO_2 \leftrightarrow R'R'R' - O - AMH^+ + HCO_3^- \quad (9)$$

This was confirmed by characterization of the nanoparticles after the absorption process. Figure 9b shows the functional groups and the chemical component of graphene oxide after the absorption using FTIR. However, the observed absorption rate enhancement is not due to the interaction between the GO and amine liquid as this interaction was observed for the nanofluids with loading higher than 0.3, 0.4, and 0.5 mg/mL, whereby the decrease in the absorption rate was observed. This may be due to the agglomeration of the nanoparticles, resulting

https://doi.org/10.1021/acsomega.3c06425
ACS Omega 2024, 9, 25625−25637

in decreased surface area and decreased Brownian motion in the solution. The increase in the absorption rate is attributed to the improved Brownian motion and increased surface area in the nanofluids with 0.1 and 0.2 mg/mL of GO loading. Brownian motion facilitated improved hydrodynamic effects and bubble-breaking effects that increased the absorption rate of absorption in the nanofluids.

3.9. Selectivity of the Nanofluids. Methane adsorption on graphene oxide nanoparticles has been studied as a method to adsorb and store methane.[48,49] Methane was not absorbed in either the prepared base fluids or nanofluids. This means that incorporating graphene oxide nanoparticles in the amine solutions did not compromise the selectivity of amine toward carbon dioxide. This can be attributed to the amine group reacting with oxygen containing a group of graphene oxide during sonication. Furthermore, methane does not possess Lewis's acid characteristics, which are possessed by carbon dioxide, which explains the low interaction between methane and amine liquids.

3.10. Influence of Methane Gas on the Absorption of CO_2. The binary gas system of CH_4 and CO_2 gases in 50:50 ratio as in contact of the amine solution and the two best-performing amine-based nanofluids. The pressure decay and absorption kinetics were observed (Figure 10). In comparison to the absorption of pure CO_2 experiments, the addition of methane in the chamber resulted in a higher absorption rate. This can be attributed to the methane gas molecules colliding with carbon dioxide gas molecules, therefore resulting in high absorption of CO_2 molecules. However, at low CO_2 concentrations, the absorption kinetics of CO_2 slows due to the presence of high CH_4 concentrations, colliding with the remaining CO_2 molecules and restricting their absorption in the amine solutions. Figure 10a shows the decaying pressure during the absorption of CO_2. Figure 10b shows the absorption kinetics of CO_2 in the amine solutions/nanofluids. It can be observed that the nanofluids showed a higher absorption rate compared to that of the 30% amine solutions.

The absorption rate constants (Table 2) show that the EDA-based solution/nanofluid showed a higher absorption rate as compared to the MEA-based solution/nanofluid the absorption rates of CO_2 in the amine solutions/nanofluids were 0.18239 for 30% EDA, 0.18351 for 30% MEA, 0.20059 for 30% EDA-0.2 mg/mL GO, and 0.18742 for 30% MEA 0.2 mg/mL. The absorption rate is higher as compared to the pure CO_2 gas system. The used amine solutions/nanofluids achieved 91.6% removal of CO_2 from the binary system.

Table 2. CO_2 Absorption Rate Constant during the Binary CH_4/CO_2 Gas System

solution type	absorption rate constant (k)
30% EDA	0.18239
30% MEA	0.18351
30% EDA 0.2 mg/mL GO	0.20059
30% MEA 0.2 mg/mL GO	0.18742

3.11. Regeneration Studies. The stability of the 30% MEA and EDA solutions and the 0.2 mg/mL GO loading MEA and EDA nanofluids was investigated to determine the decrease in absorption capacity and absorption rate. After absorption, the solvent was heated in a water bath at 90 °C for 2 h under vacuum to desorb the carbon dioxide from the solution to perform 3 absorption−desorption regeneration cycles. In comparison with fresh 30% MEA solvent (Figure 11a), it can be observed that the pressure decay for the second and third regeneration cycles reached equilibrium at 46 min, whereas the fresh solution and first cycle reached equilibrium at 36 min. The delayed reach to equilibrium was also observed in the CO_2 absorption kinetics as observed in Figure 11b. The absorption rate constant of the cycles decreased by 2.2% in the first cycle, 2.7% in the second cycle, and 5.8% in the third cycle. It can be deduced that regeneration of the amine solution did not result in a significant decrease of the absorption rate (Table 3). Therefore, this signals that the MEA solution did not chemically change due to the applied heat. The pH of the MEA solution is a good indicator of the stability of the physiochemical properties of the solution during desorption cycles. The pH of the fresh solution was 11.04, after the cycle and decreased to 10.93 for the first cycle, 10.84 s cycle, and 10.44 in the third cycle (see Table 4).

The pressure decay (Figure 12a) and CO_2 absorption kinetics (Figure 12b) of 30% MEA-0.2 mg/mL nanofluid showed the same trend as the MEA solution whereby the equilibrium of the regenerated solutions (cycles 2 and 3) reached equilibrium at 40 min, whereas the fresh solution and the first cycle reached equilibrium at 32 min. The MEA-based nanofluid with 0.2 mg/mL GO during carbon dioxide absorption during the regeneration cycles showed a higher absorption rate as compared to the 30% MEA solution. The absorption rate constant decreased by 1.3% in the first cycle, 2.7% in the second cycle, and 2.9% in the third cycle.

For the 30% fresh EDA solution (see Figure 13a,b), pressure decay and CO_2 uptake kinetics reached equilibrium at 36 min, whereas the generated 30% EDA solution reached equilibrium at 42 for the first cycle and 62 min for the second and third cycle. The absorption rate constant decreased from 0.13119 to 0.12744 in the first cycle and further decreased to 0.10937 in the second cycle and 0.10361 in the third cycle. The pH (Table 4) of the regenerated solutions decreased from 11.28 for the fresh solution to 10.65 for the first cycle, further decreased to 10.17 for the second cycle, and last 9.86 in the third cycle. The color change due to regeneration by heating was observed in the 30% EDA solution.

Figure 14a,b shows the pressure decay during the absorption experiment and the CO_2 absorption kinetics in fresh 30% EDA-0.2 mg/mL GO and regenerated 30% EDA-0.2 mg/mL. It can be observed that the pressure decay and the CO_2 uptake kinetics of the fresh EDA-based nanofluid and the first cycle reached equilibrium at 36 min while the second cycle reached equilibrium at 46 min and the third cycle at 40 min. The absorption rate constant (Table 3) decreased from 0.17603 for the absorption in the fresh solution to 0.16345 in the first cycled solution, 0.15459 in the second cycled solution, and 0.14776 in the third cycled solution. The pH of the solution also showed a decrease after regeneration, the fresh solution had a pH of 12.14, which decreased to 10.93 for the first cycle solution, 10.49 for the second cycled solution, and 10.43 for the third cycled solution (Table 4).

Comparing the behavior of MEA and EDA solution/nanofluids during the regenerated cycles. It can be observed that both EDA and MEA-based solutions/nanofluids show a reduction in the degree of regeneration for the cycles compared to the initial fresh solutions/nanofluids. During the 3 cycles using regenerated solutions the MEA-based solution/nanofluids showed a low decrease of the absorption rate constant as reported in Table 3. However, EDA showed a

https://doi.org/10.1021/acsomega.3c06425
ACS Omega 2024, 9, 25625−25637

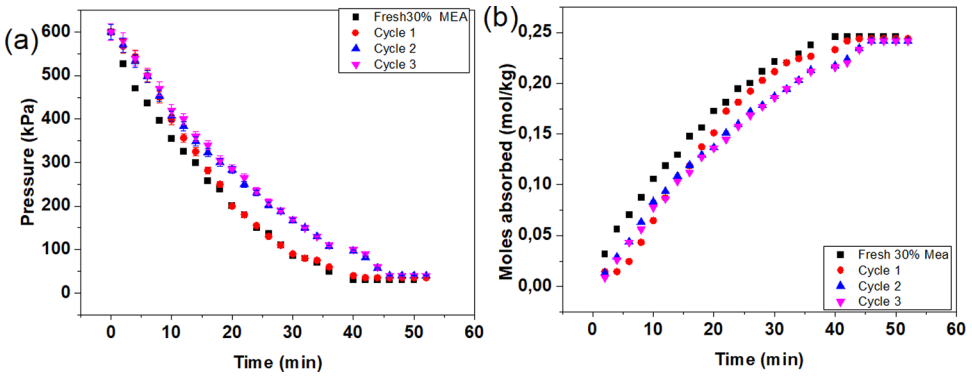

Figure 11. (a) Pressure decay and (b) CO_2 absorption kinetics of 30% MEA solution for fresh solutions and 1st, 2nd, and 3rd cycles.

Table 3. CO_2 Absorption Rate Constants for Fresh and Regenerated Solutions

amine-based solutions	fresh solution	cycle 1	cycle 2	cycle 3
30% MEA	0.11285	0.11034	0.1098	0.10623
30% MEA-0.2 mg/mL GO	0.16854	0.16626	0.16395	0.16349
30% EDA	0.13119	0.12744	0.10937	0.10361
30% EDA-0.2 mg/mL GO	0.17603	0.16345	0.15459	0.14776

Table 4. CO_2 pH of the Solutions after Regeneration

amine-based solutions	fresh solution	cycle 1	cycle 2	cycle 3
30% MEA	11.08	10.93	10.84	10.68
30% MEA-0.2 mg/mL GO	12.05	10.67	10.48	10.24
30% EDA	11.28	10.65	10.17	9.86
30% EDA-0.2 mg/mL GO	12.14	10.93	10.43	10.43

high decrease of the absorption rate constant during the 3 regenerated cycles. This shows that MEA-based solution/nanofluids showed higher chemical stability, as opposed to EDA-based solution/nanofluids.

The pH of the fresh solutions of 30% MEA, 30% MEA-0.2 mg/mL GO, 30% EDA, and 30% EDA-0.2 mg/mL were 11.08, 12.05, 11.28, and 12.14, respectively. The pH of the CO_2-loaded solutions was 8.14 for the MEA-based solution/nanofluid and 7.82 for the EDA-based solution/nanofluid and this value remained consistent throughout the cycles. However, after the regeneration of the solution through heating, the pH of the solutions obtained was lower than the initial pH. These results correspond to the ones obtained by Kamopas and Kiatsiriroat, where the authors regenerated MEA solutions for 3 cycles and obtained a consistent pH of 7.14 for the loaded solution and pH above 10 for the regenerated solution.[50] The pH values of the solutions are tabulated in Table 4.

4. CONCLUSIONS

Addition of an optimized amount of nanoparticles (GO) in amine liquids resulted in an improvement in the absorption rate and solubility of CO_2 in the nanofluids. This resulted in an enhancement of 49 and 34% for nanofluids with 0.2 mg/mL GO loading in MEA and EDA solutions, respectively. The enhancement was attributed to the Brownian motion of the nanoparticles in the amine solution. Brownian motion is important because it facilitated an improvement in the hydrodynamic effects and bubble-breaking effects in the nanofluids, resulting in an improvement in the CO_2 absorption in the nanofluids. However, EDA-based solutions/nanofluids have higher absorption rates than MEA-based solutions/nanofluids. The production of carbamate is observed in both MEA and EDA-based solutions/nanofluids, thus compromising the enhancement of the absorption capacity. The addition of the GO nanoparticles resulted in a reaction with the amine groups and the oxygen-containing groups of GO. This resulted in the formation of a zwitterion which readily reacted with

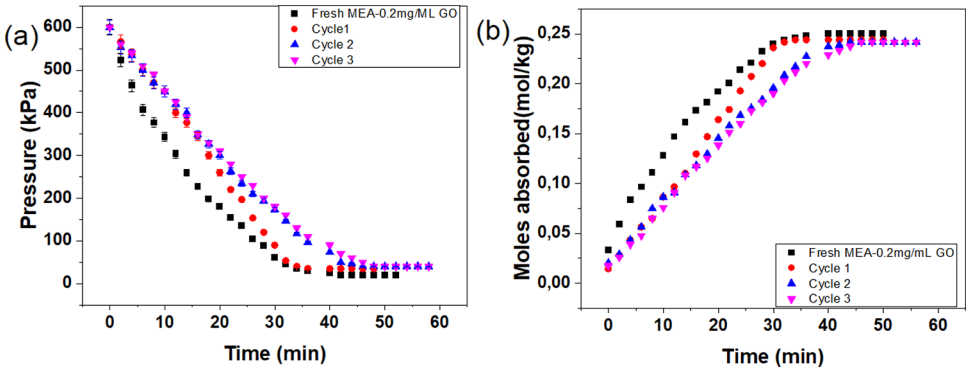

Figure 12. (a) Pressure decay and (b) CO_2 absorption kinetics of 30% MEA-0.2 mg/mL GO nanofluid for fresh solutions and 1st, 2nd, and 3rd cycles.

https://doi.org/10.1021/acsomega.3c06425
ACS Omega 2024, 9, 25625−25637

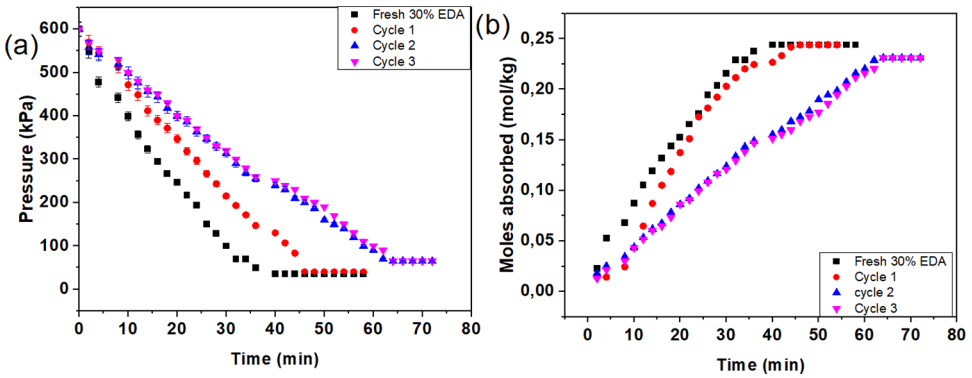

Figure 13. (a) Pressure decay and (b) CO_2 absorption kinetics of 30% EDA solution for fresh solution and 1st, 2nd, and 3rd cycles.

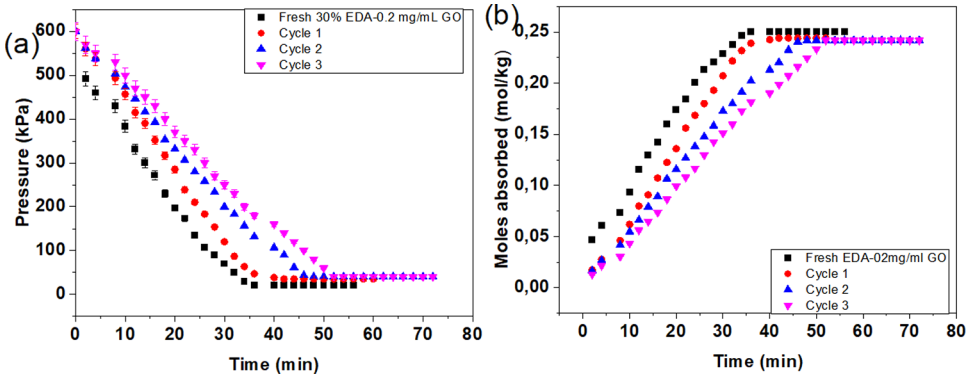

Figure 14. (a) Pressure decay and (b) CO_2 absorption kinetics of 30% EDA-0.2 mg/mL GO nanofluid for fresh solution and 1st, 2nd, and 3rd cycles.

carbon dioxide molecules, resulting in a carbamate. This was confirmed with an FTIR analysis which showed the absence of oxygen peaks and the presence of nitrogen-oxygen peaks. The BET analysis further confirmed the decrease in the surface area, pore volume, and pore diameter of the GO recovered from the nanofluids after the CO_2 experiment indicating an interaction between GO and amine molecules. The selectivity of the nanofluids was not compromised by incorporating nanoparticles in amine solutions. During mixed gas experiments, an increase in the CO_2 absorption rate was observed due to the increased kinetic speed of the molecules resulting from CO_2−CH_4 collisions. Due to the exclusive uptake of CO_2 in a mixture of methane, the proposed nanofluids can be effectively used for the purification of biogas and make these fluids ideal candidates for use in GLMC. Both MEA and EDA-based solutions/nanofluids have shown adequate chemical equilibrium stability as they were able to maintain a similar value of CO_2 loading for 3 regenerated cycles. However, a decrease in the absorption rate was noted after regeneration of the solutions/nanofluids. The nanofluids with high performance in CO_2 absorption will be used in a gas−liquid membrane contactor for CO_2 absorption.

AUTHOR INFORMATION

Corresponding Author

Machawe M. Motsa − *Institute for Nanotechnology and Water Sustainability (iNanoWS), College of Science, Engineering and Technology, University of South Africa, Florida 1709 Johannesburg, South Africa;* orcid.org/0000-0001-7315-6952; Phone: +27 11 670 9339; Email: motsamm@unisa.ac.za

Authors

Nomcebo P. Khumalo − *Institute for Nanotechnology and Water Sustainability (iNanoWS), College of Science, Engineering and Technology, University of South Africa, Florida 1709 Johannesburg, South Africa*

Oranso T. Mahlangu − *Institute for Nanotechnology and Water Sustainability (iNanoWS), College of Science, Engineering and Technology, University of South Africa, Florida 1709 Johannesburg, South Africa*

Bhekie B. Mamba − *Institute for Nanotechnology and Water Sustainability (iNanoWS), College of Science, Engineering and Technology, University of South Africa, Florida 1709 Johannesburg, South Africa;* orcid.org/0000-0003-4382-1506

Complete contact information is available at: https://pubs.acs.org/10.1021/acsomega.3c06425

Author Contributions

All the authors contributed to the manuscript conceptualization, experimental design, and editing and reviewing for submission.

Funding

This research work received financial support from the Institute for Nanotechnology and Water Sustainability and the National Research Foundation grant reference No. SRUG200406511420.

Notes

The authors declare no competing financial interest.

https://doi.org/10.1021/acsomega.3c06425
ACS Omega 2024, 9, 25625−25637

■ ACKNOWLEDGMENTS

The authors would like to acknowledge the University of South Africa and the Institute for Nanotechnology and Water Sustainability Research Unit for funding and hosting the study.

■ REFERENCES

(1) Jiang, J.; Zhao, B.; Cao, M.; Wang, S.; Zhuo, Y. Chemical Absorption Kinetics in MEA Solution with Nano-Particles. *Energy Procedia* **2013**, *37*, 518−524.
(2) Patel, H. A.; Byun, J.; Yavuz, C. T. Carbon Dioxide Capture Adsorbents: Chemistry and Methods. *ChemSusChem* **2017**, *10* (7), 1303−1317.
(3) Bengtson, G.; Neumann, S.; Filiz, V. Membranes of Polymers of Intrinsic Microporosity (PIM-1) Modified by Poly(Ethylene Glycol). *Membranes (Basel)* **2017**, *7* (2), 1−21.
(4) Bazhenov, S. D.; Bildyukevich, A. V.; Volkov, A. V. Gas-Liquid Hollow Fiber Membrane Contactors for Different Applications. *Fibers* **2018**, *6*, 4.
(5) Simons, K.; Nijmeijer, K.; Wessling, M. Gas−Liquid Membrane Contactors for CO2 Removal. *J. Membr. Sci.* **2009**, *340* (1−2), 214−220.
(6) Mansourizadeh, A.; Ismail, A. F. Hollow Fiber Gas − Liquid Membrane Contactors for Acid Gas Capture: A. *Review.* **2009**, *171*, 38−53.
(7) Li, J.; Zhang, H.; Gao, Z.; Fu, J.; Ao, W.; Dai, J. CO2 Capture with Chemical Looping Combustion of Gaseous Fuels: An Overview. *Energy Fuels* **2017**, *31* (4), 3475−3524.
(8) Baxter, L.; Baxter, A.; Burt, S. Cryogenic CO2 Capture as a Cost-Effective CO2 Capture Process; *International Pittsburgh Coal Conference, Pittsburgh, PA*, 2009
(9) Knapik, E.; Kosowski, P.; Stopa, J. Cryogenic Liquefaction and Separation of CO2 Using Nitrogen Removal Unit Cold Energy. *Chem. Eng. Res. Des.* **2018**, *131*, 66−79.
(10) Vega, F.; Cano, M.; Camino, S.; Gallego Fernández, L. M.; Portillo, E.; Navarrete, B.Solvents for Carbon Dioxide Capture; *Carbon Dioxide Chemistry, Capture and Oil Recovery*, 2018, DOI: DOI: 10.5772/INTECHOPEN.71443.
(11) Mendes, A. Determination of CO2 Absorption Kinetics in Amino Acid Salts Solutions Using Membrane Contactors. *International Journal of Membrane Science and Technology* **2017**, *4* (1), 8−18.
(12) Khodadadi, M. J.; Abbasi, M.; Riahi, S.; Shokrollahzadeh, H. Nvestigation on Kinetics of Carbon Dioxide Absorption in Aqueous Solutions of Monoethanolamine + 1, 3-Diaminopropane. *J. Membr. Sci.* **2018**, *7* (1), 1−12.
(13) Yu, W.; Wang, T.; Park, A.-H. A.; Fang, M. Review of Liquid Nano-Absorbents for Enhanced CO 2 Capture. *Nanoscale* **2019**, *11* (37), 17137−17156.
(14) Sen Gupta, S.; Bhattacharyya, K. G. Kinetics of Adsorption of Metal Ions on Inorganic Materials: A Review. *Adv. Colloid Interface Sci.* **2011**, *162* (1−2), 39−58.
(15) Zhou, J.; Wang, X.; Xing, W. *Chapter 1. Carbon-Based CO2Adsorbents*; 2018, pp. 1−75, DOI: 10.1039/9781788013352-00001.
(16) Khandaker, T.; Hossain, M. S.; Dhar, P. K.; Rahman, M. S.; Hossain, M. A.; Ahmed, M. B. Efficacies of Carbon-Based Adsorbents for Carbon Dioxide Capture. *Processes* **2020**, *8* (6), 654.
(17) Gao, W. The Chemistry of Graphene Oxide. *Graphene Oxide: Reduction Recipes, Spectroscopy, and Applications* **2015**, 61−95.
(18) Mishra, A. K.; Ramaprabhu, S. Carbon Dioxide Adsorption in Graphene Sheets. *AIP Adv.* **2011**, *1*, 32152.
(19) Politakos, N.; Cordero-lanzac, T.; Tomovska, R. Understanding the Adsorption Capacity for Co2 in Reduced Graphene Oxide (Rgo) and Modified Ones with Different Heteroatoms in Relation to Surface and Textural Characteristics. *Appl. Sci. (Switzerland)* **2021**, *11*, 20.
(20) Pruna, A. I.; Barjola, A.; Cárcel, A. C.; Alonso, B.; Giménez, E. Effect of Varying Amine Functionalities on CO2 Capture of Carboxylated Graphene Oxide-Based Cryogels. *Nanomaterials* **2020**, *10* (8), 1−15.
(21) Liu, Y.; Sajjadi, B.; Chen, W. Y.; Chatterjee, R. Ultrasound-Assisted Amine Functionalized Graphene Oxide for Enhanced CO2 Adsorption. *Fuel* **2019**, *247*, 10−18.
(22) Sun, Y.; Tang, X.; Bao, H.; Yang, Z.; Ma, F. The Effects of Hydroxide and Epoxide Functional Groups on the Mechanical Properties of Graphene Oxide and Its Failure Mechanism by Molecular Dynamics Simulations. *RSC Adv.* **2020**, *10* (49), 29610−29617.
(23) Lu, S.; Zhao, Y.; Song, J.; Li, Y. Experimental Studies of CO2 Absorption Enhancement in Water-Based Nanofluids of Carbon Nanotubes. *Braz. J. Chem. Eng.* **2019**, *34* (2), 597−606, DOI: 10.1590/0104-6632.20170342s20140144.
(24) Irani, V.; Maleki, A.; Tavasoli, A. CO2 Absorption Enhancement in Graphene-Oxide/MDEA Nanofluid. *J. Environ. Chem. Eng.* **2019**, *7* (1), 102782.
(25) Pashaei, H.; Ghaemi, A. CO2 Absorption into Aqueous Diethanolamine Solution with Nano Heavy Metal Oxide Particles Using Stirrer Bubble Column: Hydrodynamics and Mass Transfer. *J. Environ. Chem. Eng.* **2020**, *8* (5), No. 104110.
(26) Rahmatmand, B.; Keshavarz, P.; Ayatollahi, S. Study of Absorption Enhancement of CO2 by SiO2, Al2O3, CNT, and Fe3O4 Nanoparticles in Water and Amine Solutions. *J. Chem. Eng. Data* **2016**, *61* (4), 1378−1387.
(27) Devakki, B.; Thomas, S. Experimental Investigation on Absorption Performance of Nanofluids for CO2 Capture. *Int. J. Air-Condit. Refrig.* **2020**, *28* (2), No. 2050017, DOI: 10.1142/S2010132520500170.
(28) Hamdy, L. B.; Chitrakshi Goel, ab; Rudd, J. A.; Ade, Andrew Barron; Ac, R.; Andreoli, E. The Application of Amine-Based Materials for Carbon Capture and Utilisation: An Overarching View. *Mater. Adv.* **2021**, *2*, 5843.
(29) Wang, H.; Yuan, X.; Wu, Y.; Huang, H.; Peng, X.; Zeng, G.; Zhong, H.; Liang, J.; Ren, M. M. Graphene-Based Materials: Fabrication, Characterization and Application for the Decontamination of Wastewater and Wastegas and Hydrogen Storage/Generation. *Adv. Colloid Interface Sci.* **2013**, *195−196*, 19−40.
(30) Mahlangu, O. T.; Nackaerts, R.; Thwala, J. M.; Mamba, B. B.; Verliefde, A. R. D. Hydrophilic Fouling-Resistant GO-ZnO/PES Membranes for Wastewater Reclamation. *J. Membr. Sci.* **2017**, *524*, 43−55. (August 2016)
(31) Mohammadpour, A.; Mirzaei, M.; Azimi, A.; Tabatabaei Ghomsheh, S. M. Solubility and Absorption Rate of CO2 in MEA in the Presence of Graphene Oxide Nanoparticle and Sodium Dodecyl Sulfate. *Int. J. Ind. Chem.* **2019**, *10* (3), 205−212.
(32) Zhang, Z.; Schniepp, H. C.; Adamson, D. H. Characterization of Graphene Oxide: Variations in Reported Approaches. *Carbon N Y* **2019**, *154*, 510−521.
(33) Mo, Z.; Liu, H.; Hu, R.; Gou, H.; Li, Z.; Guo, R. Amino-Functionalized Graphene/Chitosan Composite as an Enhanced Sensing Platform for Highly Selective Detection of Cu2+. *Ionics (Kiel)* **2018**, *24* (5), 1505−1513.
(34) Rosnan, A.; Yeit Haan, T.; Wahab Mohammad, A. Synthesis and Characterization of ZnO-Decorated GO Nanocomposite Material with Different ZnO Loading through Sol-Gel Method. *J. Eng.* **2018**, *30* (2), 249−255.
(35) Rattana, T.; Chaiyakun, S.; Witit-Anun, N.; Nuntawong, N.; Chindaudom, P.; Oaew, S.; Kedkeaw, C.; Limsuwan, P. Preparation and Characterization of Graphene Oxide Nanosheets. *Procedia Eng.* **2012**, *32*, 759−764.
(36) Paredes, J. I.; Villar-Rodil, S.; Martínez-Alonso, A.; Tascón, J. M. D. Graphene Oxide Dispersions in Organic Solvents. *Langmuir* **2008**, *24* (19), 10560−10564.
(37) Rong, L.; Fu, Y.; Li, Q.; Yang, X.; Li, Y.; Yan, L.; Wang, L.; Wu, W. Effects of the Surface Charge of Graphene Oxide Derivatives on Ocular Compatibility. *Nanomaterials* **2022**, *12*, 5.
(38) Kashyap, S.; Mishra, S.; Behera, S. K. Aqueous Colloidal Stability of Graphene Oxide and Chemically Converted Graphene. *Journal of Nanoparticles* **2014**, *2014*, 1−6.

https://doi.org/10.1021/acsomega.3c06425
ACS Omega 2024, 9, 25625−25637

(39) Sadhukhan, S.; Ghosh, T. K.; Rana, D.; Roy, I.; Bhattacharyya, A.; Sarkar, G.; Chakraborty, M.; Chattopadhyay, D. Studies on Synthesis of Reduced Graphene Oxide (RGO) via Green Route and Its Electrical Property. *Mater. Res. Bull.* **2016**, *79*, 41−51.
(40) Alshamsi, H. A.; Ali, S. K.; Altaa, S. H. A. Green Synthesis and Characterization of Reduced Graphene Oxide (RGO) Using Sabdarriffa L Extract and Its Solubility Property. *J. Phys. Conf. Ser.* **2020**, *1664* (1), No. 012058.
(41) Yadav, K. K.; Wadhwa, R.; Khan, N.; Jha, M. Efficient Metal-Free Supercapacitor Based on Graphene Oxide Derived from Waste Rice. *Curr. Res. Green Sustain. Chem.* **2021**, *4*, No. 100075.
(42) Khumalo, N. P.; Nthunya, L. N.; De Canck, E.; Derese, S.; Verliefde, A. R.; Kuvarega, A. T.; Mamba, B. B.; Mhlanga, S. D.; Dlamini, D. S. Congo Red Dye Removal by Direct Membrane Distillation Using PVDF/PTFE Membrane. *Sep Purif Technol.* **2019**, *211*, 578−586.
(43) Gómez-Díaz, D.; Navaza, J. M.; Rumbo, A. Carbon Dioxide Chemical Absorption Using Diamines with Different Types of Active Centers. *Separations* **2022**, *9* (11), 343.
(44) Sharma, M. M. Kinetics of Reactions of Carbonyl Sulphide and Carbon Dioxide with Amines and Catalysis by Brönsted Bases of the Hydrolysis of COS. *Trans. Faraday Soc.* **1965**, *61* (0), 681−688.
(45) Ghasemi, M. H.; Irani, V.; Tavasoli, A. Amino Functionalized ZIF-90@GO/MDEA Nanofluid: As a New Class of Multi-Hybrid Systems to Enhance the Performance of Amine Solutions in CO2 Absorption. *J. Nat. Gas Sci. Eng.* **2020**, *74*, No. 103110.
(46) Salvi, A. P.; Vaidya, P. D.; Kenig, E. Y. Kinetics of Carbon Dioxide Removal by Ethylenediamine and Diethylenetriamine in Aqueous Solutions. *Can. J. Chem. Eng.* **2014**, *92* (12), 2021−2028.
(47) Hwang, G. S.; Stowe, H. M.; Paek, E.; Manogaran, D. Reaction Mechanisms of Aqueous Monoethanolamine with Carbon Dioxide: A Combined Quantum Chemical and Molecular Dynamics Study. *undefined* **2015**, *17* (2), 831−839.
(48) Taheri, Z.; Pour, A. N Studying of the Adsorption and Diffusion Behaviors of Methane on Graphene Oxide by Molecular Dynamics Simulation. *J. Mol. Model* **2021**, *27*, 59 DOI: 10.1007/s00894-021-04692-6/Published.
(49) Chouhan, R. K.; Ulman, K.; Narasimhan, S. Graphene Oxide as an Optimal Candidate Material for Methane Storage. *J. Chem. Phys.* **2015**, *143* (4), No. 044704.
(50) Kamopas, W.; Kiatsiriroat, T. Regeneration of Mono-Ethanolamine Solution After Biogas Purification by Electrical Heating with Assisted Ultrasonic Wave. *Waste Biomass Valoriz.* **2019**, *10* (12), 3879−3884.

https://doi.org/10.1021/acsomega.3c06425
ACS Omega 2024, 9, 25625−25637